PERGAMON

Journal of Quantitative Spectroscopy & Radiative Transfer 79–80 (2003) 1171–1188

Journal of Quantitative Spectroscopy & Radiative Transfer

www.elsevier.com/locate/jqsrt

The spectral signature of mixed-phase clouds composed of non-spherical ice crystals and spherical liquid droplets in the terrestrial window region

Ping Yang[a,*], He-Li Wei[a], Bryan A. Baum[b], Hung-Lung Huang[c], Andrew J. Heymsfield[d], Yong X. Hu[b], Bo-Cai Gao[e], David D. Turner[c]

[a] *Department of Atmospheric Sciences, Texas A&M University, TAMU 3150, College Station, TX 77843, USA*
[b] *NASA Langley Research Center, Hampton, VA 23681, USA*
[c] *Cooperative Institute for Meteorological Satellite Studies, University of Wisconsin 1225 W. Dayton Street, Madison, WI 53706, USA*
[d] *National Center for Atmospheric Research, Boulder, CO 8030, USA*
[e] *Remote Sensing Division, Naval Research Laboratory, Washington, DC 20375, USA*

Received 20 May 2002; accepted 4 September 2002

Abstract

An outstanding problem facing the cloud modeling and remote sensing community is to improve satellite-derived cloud microphysical and macrophysical properties when a single cloud layer exists within a temperature range for which a combination of water and ice particles may be present. This is typically known as a "mixed-phase" cloud condition, and is prevalent when the cloud-top temperature lies between −40°C and 0°C. In this paper we report on a sensitivity study of the spectral signature of mixed-phase clouds in the infrared terrestrial window region (8–13 μm). Mixed clouds are assumed to be a vertically uniform cloud layer composed of a mixture of pristine hexagonal ice crystals and spherical water droplets.

Unlike the conventional approach that derives the bulk scattering properties of mixed-phase clouds by a linear weighting of the contributions of ice and water components, the bulk single-scattering properties of mixed-phase clouds are formulated on the basis of fundamental physics. With the aid of a line-by-line radiative transfer model and a discrete ordinates radiative transfer (DISORT) computational program, we investigate the high-resolution spectral signature, expressed in terms of brightness temperature, of mixed-phase clouds with various effective sizes, ice fraction ratios, and optical thicknesses. Small particles are found to have a significant impact on the infrared spectral signature of mixed-phase clouds when the size discrepancy between the ice and water particles is large. Furthermore, the simulation results show that the infrared radiative spectrum

* Corresponding author. Tel.: +1-979- 845-4923; fax: +1-979- 862-4466.
E-mail address: pyang@ariel.met.tamu.edu (P. Yang).

0022-4073/03/$ - see front matter
doi:10.1016/S0022-4073(02)00348-5

associated with cirrus clouds can be quite different from their counterparts for cirrus clouds even if a small amount of water droplets exist in the mixed-phase cloud layer.

Keywords: Mixed-phase clouds; Single-scattering parameters; Infrared; High-resolution spectral signature

1. Introduction

Clouds typically cover a substantial portion of the globe and thus are important to the Earth's climate. They reflect solar radiation, absorb the thermal emission from the ground and lower atmosphere, and emit infrared (IR) radiation to space. An outstanding problem for the satellite remote sensing and radiative transfer communities is the treatment of mixed-phase clouds, i.e., clouds that may contain a mixture of both water and ice particles. Treut et al. [1] showed that shortwave and longwave radiative forcings are substantially different for two cloud parameterization schemes developed for mid-level, mixed-phase clouds. Other studies [2,3] have also shown the importance of mid-level, mixed-phase clouds on the radiation budget. Additionally, mixed-phase clouds have implications for aviation safety. Riley [4] discussed possible safety hazards due to flight in mixed-phase conditions, which lead to aircraft icing, and suggested that aircraft may be traveling through mixed-phase clouds at least 20% of the time.

Current operational satellite retrieval efforts typically assume that clouds are either completely liquid or ice phase. Because of a lack of observational datasets until recently, there has been much uncertainty regarding the composition of clouds that reside at temperatures between $-40°C$ (the homogeneous nucleation temperature) and $0°C$. In fact, mixed-phase conditions in the atmosphere are common. Observations recorded over a four-month period by Shupe et al. [5] in the Arctic show that only about 34% of all cases are pure ice clouds or pure liquid clouds. The remaining cases are essentially mixed-phase clouds with coexisting ice particles and liquid droplets. Pinto et al. [6] and Girard and Curry [7] observed an abundance of mixed-phase clouds in the Arctic that occurred over a broad temperature range from $-34°C$ to $-5°C$. As satellite-borne cloud retrieval products are derived under the assumption that clouds are composed entirely of either water or ice particles, mixed-phase clouds pose a problem that deserves attention. We note that no current global cloud product analyses support operational retrieval of cloud macrophysical or microphysical properties when both water and ice are present.

Young et al. [8] used the lidar-radiometer (LIRAD) method to provide detailed information on the IR emittance of clouds [9] during the Experimental Cloud Lidar Pilot Study (ECLIPS) in 1989 (ECLIPS I) and 1991 (ECLIPS II) in Aspendale, Australia. Young et al. [8] also presented a number of cases of mid-level clouds observed in 1991 as part of ECLIPS II, wherein the cloud temperatures ranged from $-25°C$ to $0°C$. The ice phase tended to dominate at temperatures below $-20°C$, while at temperatures between $-20°$ and $-5°C$, water and ice were identified in roughly equivalent amounts (note that the depolarization lidar was used to determine the dominant phase).

Hogan et al. [10,11] have documented the characteristics of mixed-phase clouds from the 1998 Cloud Lidar and Radar Experiment (CLARE) as observed by a suite of ground-based and airborne instruments. In their two case studies, the lidar returns were sensitive to the presence of supercooled

water droplets, while the radar echoes were dominated by the presence of large ice particles. The water droplets were found to have small effective radii, ranging from 2 to 5 μm. The supercooled water clouds tended to occur in geometrically thin (100–200 m) layers. Hexagonal ice plates were found to grow quickly within the cloud layer. Robert and Tokay [12] explained the existence of supercooled water at the top of cold clouds. Although some observations of mixed-phase clouds have been conducted by using lidar or radar facilities [13], relatively less effort has been focused on the issue regarding the spectral radiative effect of mixed-phase clouds.

In this study, we focus our attention on the inference of mixed-phase cloud properties in the IR window region. Atmospheric radiation in the IR atmospheric windows region contains a wealth of information that may be useful for the retrieval of cloud properties. For the remote sensing of cloud properties, the use of IR spectral radiance has some prevailing advantages over the use of visible and near-infrared bands. First, it is usually problematic to detect and analyze optically thin (or subvisual) clouds at visible or near-infrared wavelengths with an exception of 1.38 μm spectral band that is particularly effective for retrieving thin cirrus reflectance [14]. Thin clouds tend to be radiatively important in IR region because of strong absorption [15]. Second, an IR analysis approach may be employed operationally regardless of solar viewing conditions (i.e., both day and night). It has been demonstrated that high-spectral resolution interferometric measurements can be used to retrieve both cloud altitude [16] and cloud properties [17]. However, previous retrieval efforts have assumed that clouds are either in liquid or ice phase.

While mixed-phase clouds may occur quite frequently in both hemispheres at higher latitudes, there is very little discussion on this issue in the scientific literature. The intent of the present study is first to formulate the bulk single-scattering properties of mixed-phase clouds based on those derived for the polydisperse systems composed of either ice crystal or water droplets. It is well known that cirrus clouds are composed of ice crystals with a variety of shapes. Because this paper is mainly concerned with the sensitivity of IR spectral radiative signature of mixed-phase clouds, we simplify the issue by assuming that mixed-phase clouds are composed of a uniform mixture of pristine hexagonal ice crystals and spherical water droplets. Second, the single-scattering properties of mixed-phase clouds and their dependence on effective size and the ratio of ice water content (IWC) to total water content (TWC) are discussed. Finally, with the use of a line-by-line (LBL) radiative transfer code and the discrete ordinate radiative transfer (DISORT) [18] method, we investigate the high-resolution IR spectral brightness temperatures for various mixtures of ice crystal and water droplets. These results are compared subsequently to the cases for pure ice or pure water clouds.

2. Single-scattering properties of mixed-phase clouds: basic formulation

To retrieve cloud properties from satellite- and aircraft-borne measurements, the absorption and scattering properties of clouds, and in particular their spectral variation, must be known. The particles in liquid water clouds can be well approximated as liquid spheres, and their optical properties can be computed using the Lorenz–Mie theory [19]. In this study we computed the optical properties for liquid water clouds using the computational code developed by Wiscombe [20] by assuming a gamma size distribution. Various in situ observations have demonstrated that cirrus clouds consist of non-spherical ice crystals [e.g., [21,22]]. A number of studies [e.g., [23–25]] have computed single scattering properties for ice crystals at IR wavelengths, demonstrating that the non-sphericity of ice

crystals can substantially affect the optical properties of these particles. In the present study the scattering and absorption properties of hexagonal ice crystals were calculated using a combination of the finite-difference time-domain (FDTD) technique and the stretched scattering potential method (SSPM) for sizes ranging from 1 to 1000 μm, which has been reported by Yang et al. [25].

Let us consider a mixed-phase cloud that is assumed to be an externally uniform mixture of ice and water particles. The extinction coefficient, β_e, of the mixed-phase cloud is the sum of the contributions of water and ice components, given by

$$\beta_e = \int_{L_{min}}^{L_{max}} Q_{ei} A_i n_i dL + \int_{r_{min}}^{r_{max}} Q_{ew} A_w n_w dr = \frac{3}{2} \langle Q_{ei} \rangle \frac{IWC}{D_{ei} \rho_i} + \frac{3}{2} \langle Q_{ew} \rangle \frac{LWC}{D_{ew} \rho_w}, \tag{1}$$

where Q_e is the extinction efficiency, A is the projected area of the particle, n is the number density, ρ is the mass density, and the subscripts i and w denote ice and liquid particles, respectively. In Eq. (1) the mean extinction efficiency $\langle Q_e \rangle$, effective size D_e, and the ice water content IWC are given by

$$\langle Q_{ei} \rangle = \frac{\int_{L_{min}}^{L_{max}} Q_{ei} A_i n_i dL}{\int_{L_{min}}^{L_{max}} A_i n_i dL}, \tag{2}$$

$$D_{ei} = \frac{3}{2} \frac{\int_{L_{min}}^{L_{max}} V_i n_i dL}{\int_{L_{min}}^{L_{max}} A_i n_i dL}, \tag{3}$$

$$IWC = \rho_i \int_{L_{min}}^{L_{max}} V_i n_i dL, \tag{4}$$

where L is the characteristic length of ice crystals. In the case for a water component, D_{ew}, LWC, and $\langle Q_{ew} \rangle$ can be defined in a manner similar to that for the ice component of the mixed-phase cloud.

The effective size of a polydisperse cloud particle system provides a measure of the average size of the cloud particles for a given size distribution. The effective size for water droplets with a specific size distribution can be defined as the ratio of the third moment to the second moment of particle radius for the polydisperse particle system [26], as water droplets are usually modeled as spherical particles. Unlike water droplets, ice particles are not spherical. There are various ways to define the effective size of ice crystals (D_{ei}). Grenfell and Warren [27] found that representing each ice particle by a collection of independent spheres with the same ratio of volume to surface-area as the individual ice particles is a better approach than using the "equivalent" spheres defined in terms of equal-volume or equal-area. More commonly, the effective size of non-spherical particles is defined on the basis of the ratio of total volume to total projected-area [25,28–31].

We denote the TWC, ice fraction (γ), and effective density (ρ_e) of the mixed-phase cloud as follows:

$$TWC = IWC + LWC, \tag{5}$$

$$\gamma = \frac{IWC}{TWC}, \tag{6}$$

$$\frac{1}{\rho_e} = \frac{\gamma}{\rho_i} + \frac{1-\gamma}{\rho_w}. \tag{7}$$

It can be shown (see appendix) that the effective size of the mixed-phase cloud, D_e, is exactly given as follows:

$$\frac{1}{D_e} = \left(\frac{\gamma}{D_{ei}\rho_i} + \frac{1-\gamma}{D_{ew}\rho_w}\right)\rho_e. \tag{8}$$

Evidently, the effective size of a mixed-phase cloud is given by the effective sizes associated with the ice and water components, ice fraction, and the effective density. Note that Eq. (8) is mathematically exact, and avoids the error associated with the ad hoc weighting procedure in the conventional way for evaluating the effective size of mixed-phase cloud particles. Through substitution of D_e into Eq. (1) and with the definitions of TWC, γ, and ρ_e, a simple formulation for the extinction coefficient can be derived:

$$\beta_e = \frac{3}{2}\langle Q_e\rangle \frac{TWC}{D_e\rho_e}, \tag{9}$$

where the mean extinction efficiency $\langle Q_e\rangle$ is given by

$$\langle Q_e\rangle = \langle Q_{ei}\rangle \frac{D_e\rho_e\gamma}{D_{ei}\rho_{ei}} + \langle Q_{ew}\rangle \frac{D_e\rho_e(1-\gamma)}{D_{ew}\rho_{ew}}. \tag{10}$$

Similarly, the mean absorption efficiency $\langle Q_a\rangle$ can be defined as

$$\langle Q_a\rangle = \langle Q_{ai}\rangle \frac{D_e\rho_e\gamma}{D_{ei}\rho_{ei}} + \langle Q_{aw}\rangle \frac{D_e\rho_e(1-\gamma)}{D_{ew}\rho_{ew}}. \tag{11}$$

Note also the similarity of the extinction coefficient for the mixed-phase cloud (Eq. (9)) and those for single (ice or water) phase clouds [which are represented by the two terms in Eq. (1)]. From these definitions, a simple form of the asymmetry parameter for mixed-phase clouds $\langle g_e\rangle$ can be obtained (see appendix for details):

$$\langle g_e\rangle = \langle g_i\rangle \frac{(\langle Q_{ei}\rangle - \langle Q_{ai}\rangle)D_e\rho_e\gamma}{(\langle Q_e\rangle - \langle Q_a\rangle)D_{ei}\rho_{ei}} + \langle g_w\rangle \frac{(\langle Q_{ew}\rangle - \langle Q_{aw}\rangle)D_e\rho_e(1-\gamma)}{(\langle Q_e\rangle - \langle Q_a\rangle)D_{ew}\rho_{ew}}. \tag{12}$$

In Eqs. (9)–(12), the mean scattering efficiencies, extinction coefficient, asymmetry parameter, and effective size are defined in a rigorous manner without introducing any error. Additionally, these quantities for mixed-phase clouds are expressed exactly as functions of the single scattering properties of ice and water. Thus, the present formulation allows the single scattering properties of mixed-phase clouds to be computed directly from those of ice crystals and water droplets. Furthermore, existing parameterization schemes of the bulk optical properties of ice and water clouds can be employed to derive the bulk optical properties of mixed-phase clouds in a straightforward manner.

3. Single-scattering properties of mixed-phase clouds: sensitivity to microphysical variations

The derivation of the single scattering properties in the previous section allows us to investigate how the radiation field is modulated as the microphysical configuration of the mixed-phase cloud is

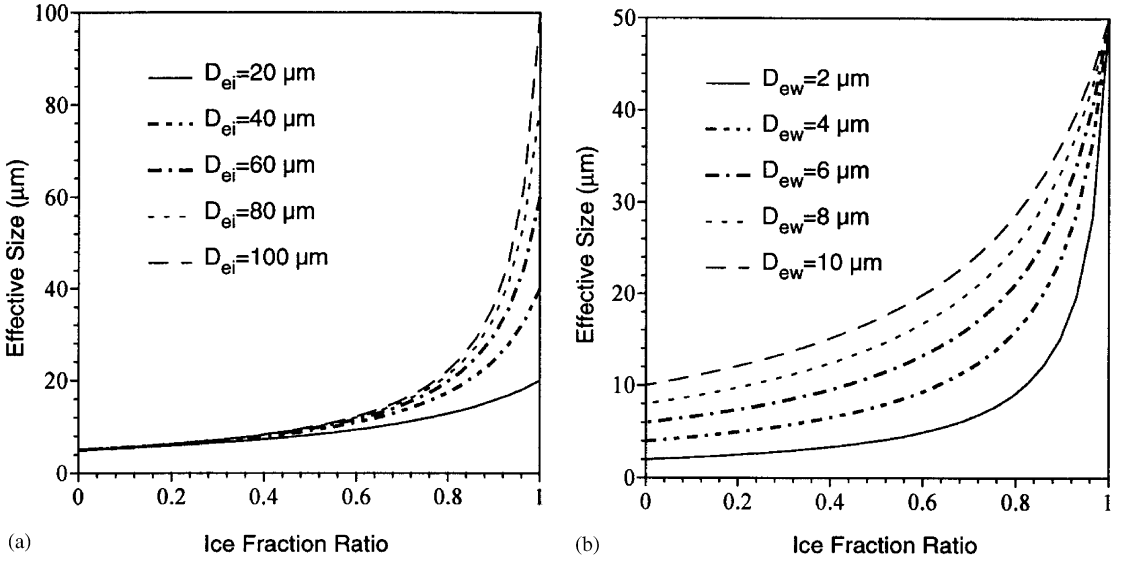

Fig. 1. The variations of the effective size D_e of mixed-phase clouds vs. the ice fraction ratio fraction γ. (a) $D_{ew} = 5.0$ μm, $D_{ei} = 20, 40, 60, 80, 100$ μm, (b) $D_{ei} = 50.0$ μm, $D_{ew} = 2, 4, 6, 8, 10$ μm.

altered. Fig. 1 shows the effective size of mixed-phase clouds particles and their variations vs. the size of ice crystal (D_{ei}), water droplets (D_{ew}), and the fraction of ice γ. As indicated in Fig. 1, the effective size of mixed-phase clouds is between the size of D_{ei} and D_{ew} and varies smoothly with the parameter γ. When $\gamma = 0$, the mixture is entirely liquid water and D_e is exactly D_{ew}; when $\gamma = 1$, the cloud is entirely ice and D_e reduces to D_{ei}. The formulation given by Eq. (8) for the effective size gives the smaller particles more weight. For example, when $\gamma = 0.5$, the effective size of mixed-phase clouds always tends towards the smaller size rather than the mean value. This is expected, as the number of small particles is much larger than the number of large ones when $\gamma = 0.5$.

Fig. 2 presents the mean extinction efficiency, absorption efficiency, and asymmetry factor for different sizes of ice crystals ($D_{ei} = 12, 25$, and 50 μm) within the spectral range 8–13 μm. The calculations for Fig. 2 were performed using the parameterization scheme developed by Yang et al. [25] on the basis of the optical properties of ice crystals associated with 30 in situ size distributions. The mean extinction efficiency of ice crystals depends strongly on wavelength, particularly for small particle sizes in the spectral region 10–12 μm. An extinction minimum at approximately 10.5 μm is noted, which corresponds to the Christiansen band of ice [32,33]. This extinction minimum becomes deeper as crystals become smaller. Because of the Christiansen effect, there is a spectral signature associated with cirrus clouds in the atmospheric window region. For a large particle sizes ($D_{ei} = 50$ μm), the spectral variation of the extinction efficiency is relatively smooth. As the sum of scattering and absorption effects, the total extinction efficiency of ice crystals in 8–9.5 μm spectral region is nearly independent of particle size. This feature is useful to the retrieval of cirrus optical thickness.

The bulk absorption efficiency of cirrus clouds are related to the imaginary component of the refractive index of ice. In addition, the absorption of ice crystals depends on wavelength and the

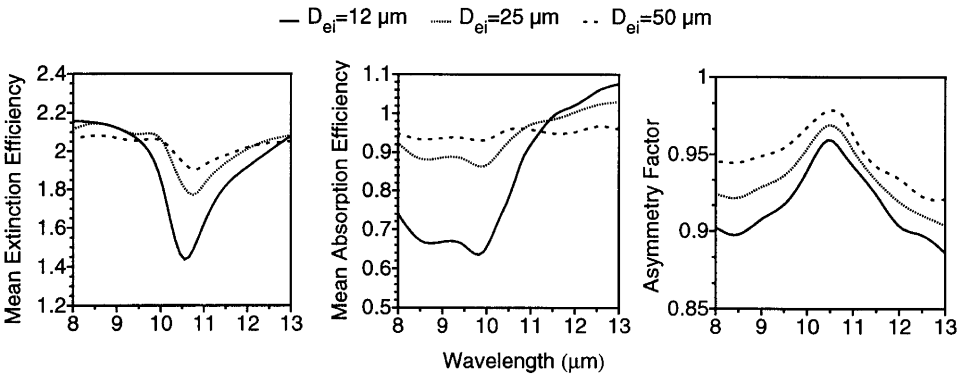

Fig. 2. Mean extinction efficiency, absorption efficiency, and asymmetry factor for various effective sizes of ice crystals ($D_{ei} = 12, 25,$ and 50 μm).

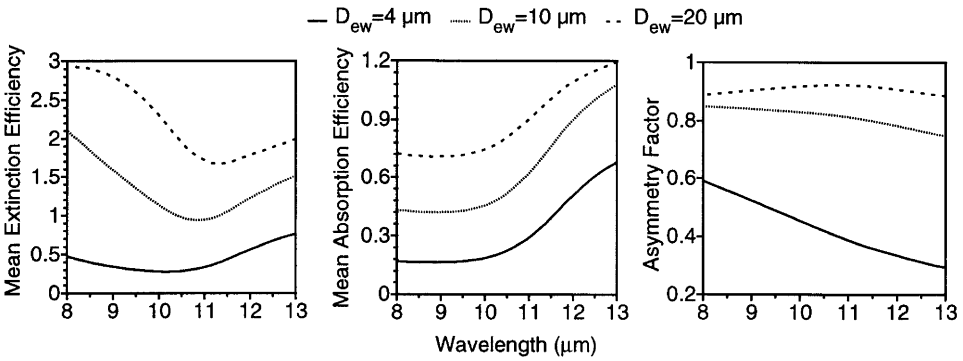

Fig. 3. Mean extinction efficiency, absorption efficiency, and asymmetry factor for various effective sizes of water droplets ($D_{ew} = 4, 10,$ and 20 μm).

effective size of the particles, as is shown in Fig. 2. The absorption efficiency has a rapid variation with wavelength in the 10–12 μm spectral region, particularly for small ice particles. This feature is useful for determining the effective size of ice crystals in cirrus clouds by using high-resolution IR atmospheric spectral measurements. The asymmetry factor for cirrus is quite large (> 0.9) in the atmospheric window, implying that the scattering of the incident radiation by ice crystals in the IR region is typically in forward direction.

Fig. 3 shows the single scattering properties for water droplets using various effective sizes at wavelengths across the atmospheric window from 8 to 13 μm. Compared to the single scattering properties of ice crystals in Fig. 2, the spectral variation of the extinction efficiency for water clouds is much smoother, particularly for small particle sizes. The asymmetry factor for water clouds is smaller and its spectral variation is smoother than for ice clouds. The absorption efficiencies are different for ice and water clouds due to the different imaginary parts of the refractive indices for ice and water.

From Eqs. (10)–(12), it is evident that the single scattering properties of mixed-phase clouds are functions of the scattering properties of the ice crystals and water droplets, their sizes, and ice

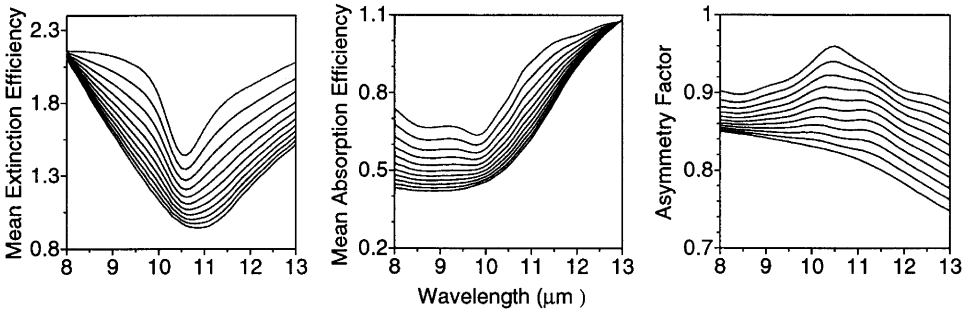

Fig. 4. The variation of single-scattering parameters of mixed-phase clouds for the atmospheric window as a function of the parameter γ, where $D_{ei} = 12$ μm, $D_{ew} = 10$ μm, and $\gamma = 1.0, 0.9, 0.8, \ldots 0.1, 0.0$ (from top curve to bottom).

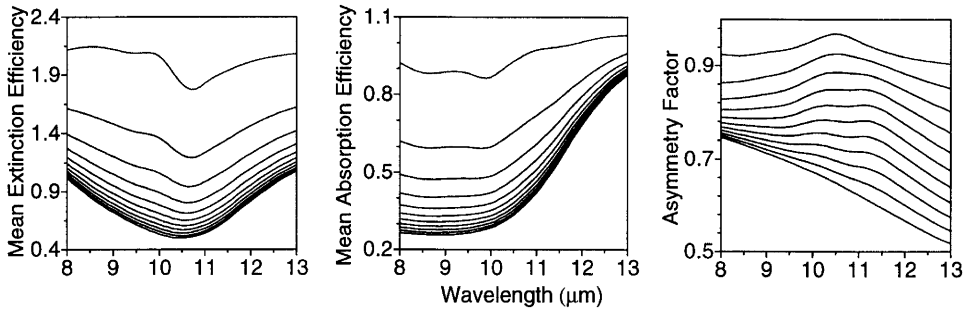

Fig. 5. Same as Fig. 4, except $D_{ei} = 25$ μm, $D_{ew} = 6$ μm.

fraction ratio. Fig. 4 shows the variation of the mean single-scattering parameters of mixed-phase particles with respect to the parameter γ and wavelength. It can be seen that the mean extinction efficiency, absorption efficiency and asymmetry factor of mixed-phase particles vary between the values for ice phase and liquid phase. When γ is 1, the single scattering properties of mixed-phase clouds reduce to that of ice, as one of the curves in the Fig. 2. Conversely, the single scattering properties of mixed-phase clouds reduce to that of water droplets if γ approaches 0. For other values of γ, the single scattering properties of mixed-phase clouds vary smoothly between those for the ice and water components. It is interesting to note in Fig. 4 that 12 μm ice crystals and 10 μm water particles have almost the same extinction efficiency at a wavelength of 8 μm and the same absorption efficiency at a wavelength of 13 μm.

Fig. 5 is the same as Fig. 4, except that the size difference between the ice and water particles is larger (19 μm in Fig. 5 vs. 2 μm in Fig. 4). Compared to Fig. 4, it is seen that the single scattering properties of mixed-phase clouds have more rapid variations with γ due to the larger size difference of the two phases. For example, when γ varies from 1.0 to 0.9, the variation of extinction and absorption efficiency is almost 40% of the total change (from $\gamma = 0$ to 1); however, when γ varies from 0.1 to 0, the variation of extinction (and also absorption) efficiency is less than 5% of the total change. This implies that the small size particles have more contribution to the variations in the single scattering properties of mixed-phase clouds at these wavelengths.

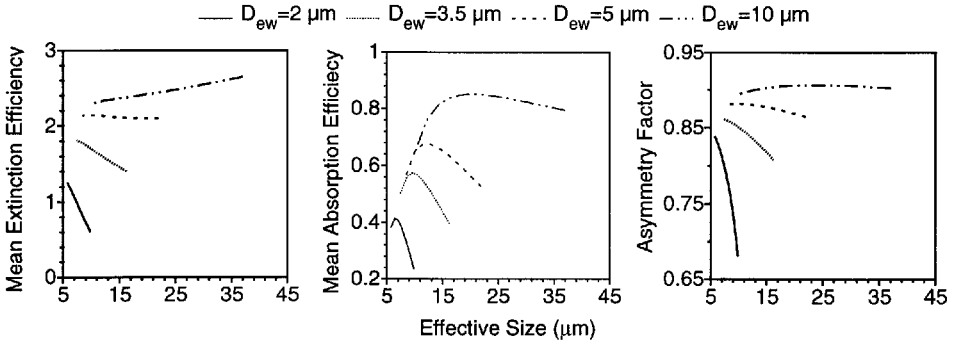

Fig. 6. The variation of single-scattering parameters vs. the effective size D_e, for $\gamma = 0.8$ and wavelength 8 μm. D_{ei} varies from 10 to 100 μm for each curve (for each curve D_{ew} is fixed).

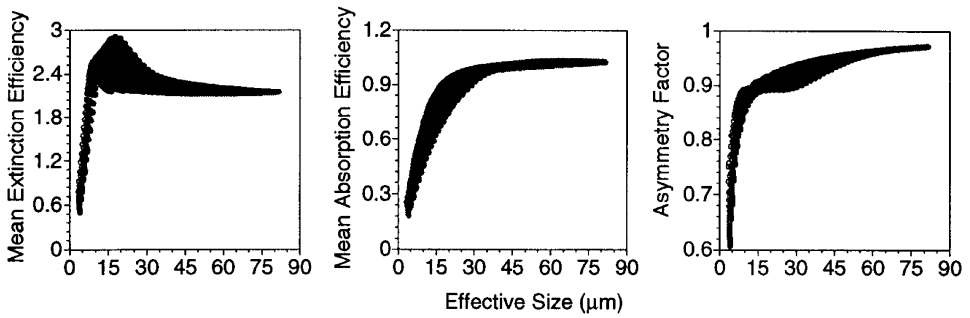

Fig. 7. The variation of single-scattering parameters vs. the effective size D_e for wavelength 8 μm (D_{ei} varies from 10 to 180 μm, and D_{ew} varies from 2 to 50 μm with $\gamma = 0.5$).

Figs. 6 and 7 show the variation of the single-scattering parameters as the effective size D_e changes. Unlike the ice or water droplets, the single scattering properties of mixed-phase particles are not unique for a specific effective size D_e (e.g., Fig. 4). Instead, the scattering properties are determined by the single scattering properties of both ice crystals and water droplets, the effective sizes of these particles, and the fractional ratio of the ice component. Therefore, the relationship among these factors is quite complex, and further study is necessary to fully understand the relationship among them.

Fig. 7 shows a scatterplot of the single-scattering parameters of mixed-phase clouds for a fixed ice fraction ratio ($\gamma = 0.5$) when D_{ei} varies from 10 to 180 μm and D_{ew} varies from 2 to 50 μm. Although the single-scattering parameters are not uniquely determined by effective size D_e, the single scattering parameters of mixed-phase clouds are strongly dependent on D_e. When $\gamma = 0$ or 1, the scatter-plot in Figs. 6 and 7 will reduce to a curve for water droplets or ice crystals in which the single-scattering properties are uniquely determined by the effective size of the particles.

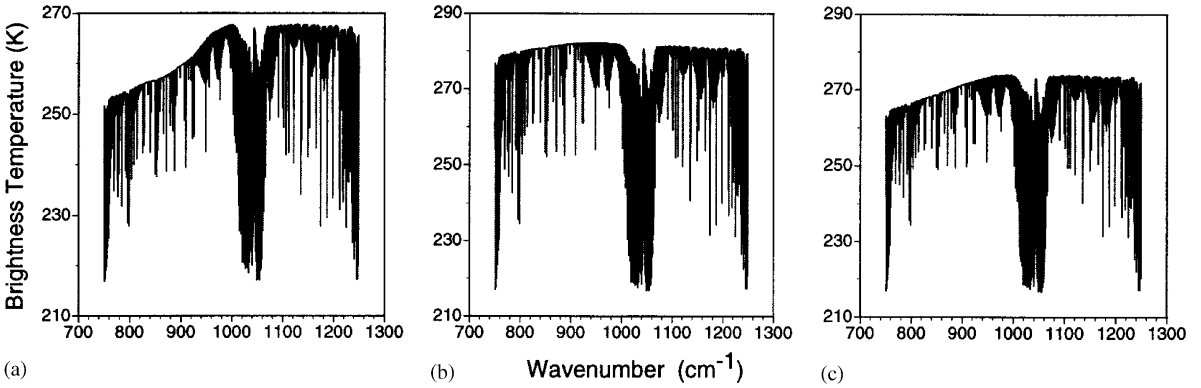

Fig. 8. The brightness temperature of 'typical' cirrus, water clouds and mixed-phase clouds. (a) Cirrus cloud: $D_{ei} = 12$ μm, cloud base height 10.0 km, thickness 0.8 km, optical thickness 1.0 when $Q_e = 2.0$. (b) Water cloud: $D_{ew} = 10$ μm, cloud base height 2.0 km, thickness 1.0 km, optical thickness 100. (c) Mixed-phase cloud: $D_{ew} = 10$ μm, $D_{ei} = 12$ μm, $\gamma = 0.5$ (resulting in $D_e = 10.95$ μm) cloud base height 8.0 km, thickness 1.0 km, optical thickness 1.0 when $Q_e = 2$.

4. IR (8–13 μm) spectral signature of mixed-phase clouds

To investigate the spectral signature of mixed-phase clouds in the atmospheric terrestrial window, upwelling brightness temperatures (BTs) are calculated at aircraft level (20 km) using the DISORT code and the single scattering properties of ice clouds, water clouds and mixed-phase clouds as defined in Section 2. The optical thicknesses of the clear sky atmosphere layers are computed with a LBL radiative transfer model, accounting for the radiatively important gases in the atmosphere (i.e., H_2O, CO_2, O_3, N_2O, HNO_3, CH_4, etc.). The line parameters are taken from HITRAN-2000 [34]. The continuum absorption of water vapor within 8–13 μm is considered by using the parameterization of Roberts et al. [35]. The spectral resolution used in the present IR radiative transfer calculation is 0.01 cm^{-1}.

The US standard atmospheric profiles (including profiles of temperature, pressure, water vapor and ozone) are used in the LBL calculations. The profiles of other trace gases are assumed to have a constant mixing ratio at every level. The atmosphere is interpolated into 100 layers below 30 km. The cloud temperature is assumed to be the same as the atmospheric temperature at that level. The surface is assumed as a blackbody (emissivity is 1) with temperature of 288.15 K.

Fig. 8 shows the brightness temperatures of "typical" cirrus (with small ice crystals), water clouds, and mixed-phase clouds as observed at the altitude of 20 km (aircraft level). Even in the 8–13 μm atmospheric window spectral region, many strong absorption lines are observed due to the gases in the atmosphere. The primary absorbing gases in this wavelength region are H_2O, O_3, and CO_2, with minor absorption by other trace gases such as CH_4 and N_2O. If an atmospheric layer is completely opaque at a certain wavenumber due to the presence of strong absorption by a trace gas, the BT at that wavenumber is largely unaffected by the cloud. Otherwise, the BT at a given wavelength is the combination of transmitted radiation from the surface, the atmosphere, and the clouds.

A comparison between the BTs of small particle cirrus and water clouds in Fig. 8 reveals some remarkable differences in their spectral features. The overall pattern (i.e., without accounting for the minima caused by absorption lines) of the BTs of water clouds is almost independent of wavelength,

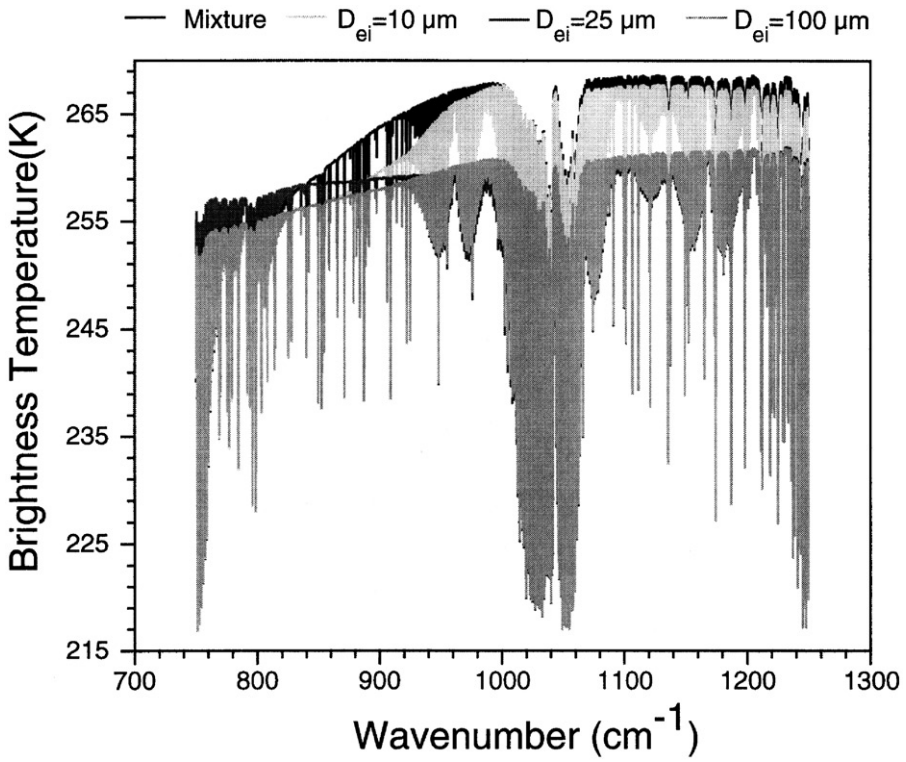

Fig. 9. BT spectra for 3 cirrus clouds and 1 mixed-phase cloud. Cloud base height: 8.0 km, thickness 1.0 km, optical thickness 1.0 when $Q_e = 2$. Cirrus clouds: $D_{ei} = 10, 25$, and 100 μm, mixed-phase cloud: $D_{ei} = 25$ μm, $D_{ew} = 10$ μm, $\gamma = 0.5$ (yielding $D_e = 14.56$ μm).

but the overall pattern of the BTs of cirrus clouds varies significantly with wavenumber between 750 and 1000 cm^{-1}. This behavior may be explained by the different extinction efficiencies of water droplets and ice crystals. Fig. 2 shows that the extinction efficiency is strongly wavelength dependent for small ice crystals. Although the extinction efficiency of water clouds has a smooth variation with wavelength, Fig. 8b shows almost no variation with respect to wavelength because of the large optical thickness of the water cloud that prevents radiation from the surface from being observed. Therefore, shown in Fig. 8b is a combination of the thermal radiation of water clouds and the atmospheric radiation above the clouds where the radiation of the cloud looks like a blackbody with the temperature of the cloud.

The radiative signature of mixed-phase clouds in Fig. 8c is different from those of the cirrus and water clouds. The overall pattern of the BT spectrum of the mixed-phase cloud within the atmospheric window is smoother than that of small-particle cirrus, yet not as flat as that of the opaque water cloud. This signature is the result of scattering and absorption properties of mixed-phase clouds that vary with the microphysical properties such as the effective size D_e, and fraction of ice γ.

Fig. 9 shows the BT spectra for cirrus clouds with different effective sizes D_{ei}. The BTs of a mixed-phase cloud are also provided for comparison. The spectral variations of the BTs from 800 to 1000 cm^{-1} show a rapid increase with wavenumber for small ice particles. The amplitude of the

slope within the wavelength range increases with decreasing ice particle size. This effect was noted as a "S" shape of cirrus forcing by Chung et al. [36] and was reported previously by Smith et al. [15]. This structure is useful for retrieval of the small ice particle sizes that sometimes occur in cirrus on the basis of IR spectral radiance measurements. The BT spectrum from 1060 to 1250 cm^{-1} is less sensitive to the effective sizes of ice crystals than to the optical thickness. Therefore, the spectral radiance of cirrus within this wavelength region is useful for retrieving the optical thickness of cirrus clouds. When the ice crystal and water droplets coexist, the radiative signature changes significantly.

The absorption lines in Figs. 8 and 9 are due to the absorption of gases such as water vapor, ozone, carbon dioxide and other trace gases. To retrieve the properties of clouds from the high-resolution spectral measurements, we are not interested in the detailed absorption lines of atmospheric molecules, which vary drastically with wavelength. Therefore, we use the radiance observations in narrow micro-windows that have relatively few gaseous absorption lines and are dominated by the radiance from clouds. By using microwindows across the spectrum, the spectral "profile" of the cloud can be found. We will discuss the variations of IR spectral signature of mixed-phase clouds to the microphysical parameters of ice and water droplets within 40 microwindows between 750 and 1250 cm^{-1} for the remainder of the paper.

Fig. 10 shows the variations of the BT spectra for mixed-phase clouds as the parameter γ changes. The fluctuations around 1050 cm^{-1} are due to the influence of ozone absorption in the 9.6 μm band where no atmospheric windows could be found. When $\gamma=0$, the cloud consists totally of liquid water droplets, and the BT spectrum for this case reflects that. Similarly, when $\gamma = 1$, the BT spectrum corresponds to that of an all-ice particle cloud. For other values of γ, the BT spectra are between those for ice and water clouds.

Consider the case of two cloud layers, one of ice and one of water, with both layers having the same visible optical thickness. If the water cloud contains a high number of small particles, the IR optical thickness (e.g., at 1000 cm^{-1}) of that layer will be lower than the ice cloud due to the extinction efficiencies. The result is that the BT of the water cloud layer will be higher than that of ice clouds.

Fig. 11 shows the variations of the BT spectrum of mixed-phase clouds as a function of the optical thickness. As expected, the BT spectrum is quite sensitive to optical thickness, as the BT decreases by 12–20 K when the optical thickness varies from 0.1 to 1. The reason is that the BT spectra of both ice and water clouds are sensitive to optical thickness. The BTs are more sensitive to the optical thickness when the clouds are located at a higher altitude (i.e., at a colder temperature).

Figs. 12 and 13 show the variations of the BT spectra of mixed-phase clouds for various effective sizes. The variation patterns are very complicated because the scattering and absorption properties of mixed-phase clouds are not uniquely determined by the effective size. These variations are related to the sizes of the ice crystals, water droplets, and the fraction ratio of ice, as well as the single-scattering properties of ice crystals and water droplets.

Compared to Fig. 9, the spectral signature of the mixed-phase cloud changes significantly when small liquid-phase particles are mixed with the pure ice particles. As is evident from Fig. 12, the smallest water droplets make a larger contribution to the BTs of the mixed-phase clouds. Because of the smaller extinction efficiency of water clouds in the IR (see Figs. 2 and 3), the optical thickness of the mixed-phase clouds is smaller than that of ice-only clouds. The larger the effective size of ice particles, the smaller the optical thickness of mixed-phase clouds when the ice fraction γ is kept constant. For this reason, mixed-phase clouds with large ice particles have a smaller optical thickness

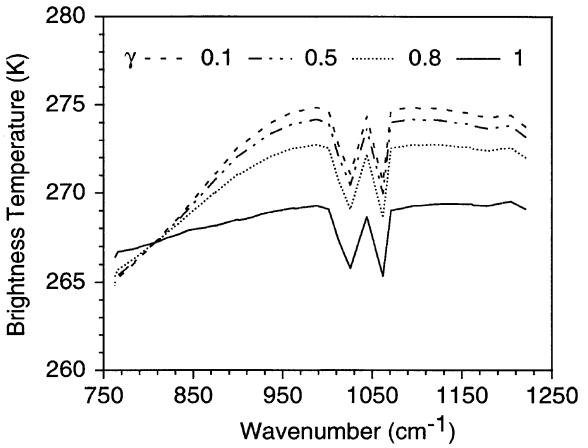

Fig. 10. The BT spectra of mixed-phase clouds (D_{ew} = 10 μm, D_{ei} = 40 μm, γ = 0.1, 0.5, 0.8, and 1.0, cloud base height 6.0 km, physical thickness 1.0 km, optical thickness 1.0 when $Q_e = 2$).

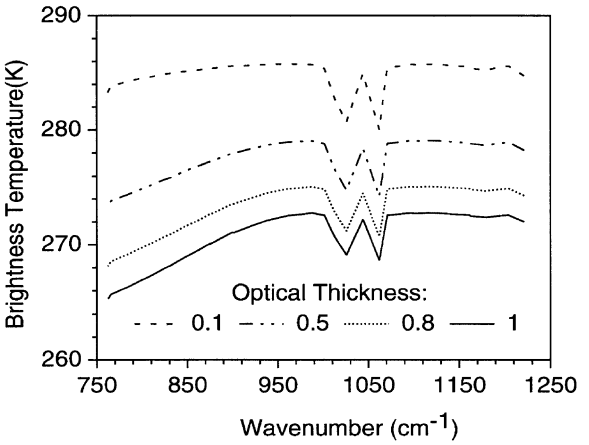

Fig. 11. Variations of the BT spectra of mixed-phase clouds as a function of optical thickness. (D_{ew} = 10 μm, D_{ei} = 40 μm, γ = 0.8, D_e = 17.36 μm, cloud base height 6.0 km, physical thickness 1.0 km, optical thickness ranges over 0.1, 0.5, 0.8, 1.0 when $Q_e = 2$).

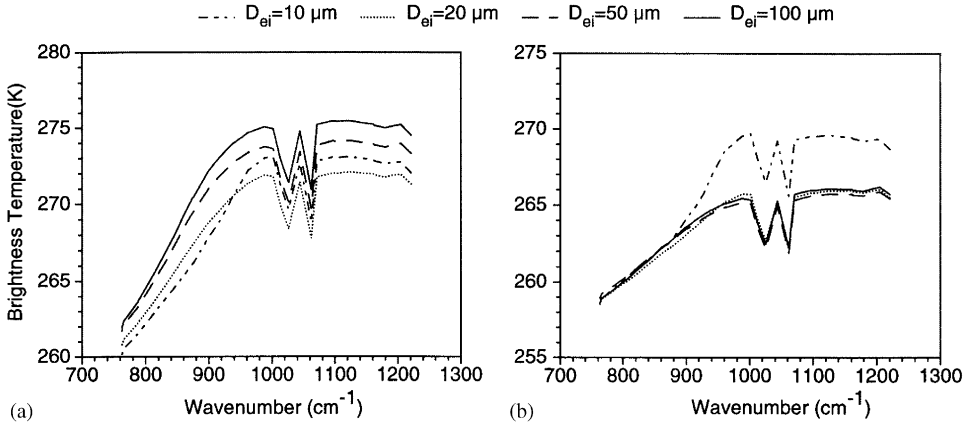

Fig. 12. The spectral variations of the BT for mixed-phase clouds vs. the effective size. Cloud base height 8.0 km, thickness 1.0 km, optical thickness = 1.0 when $Q_e = 2.0$, $\gamma = 0.8$, $D_{ei} = 10, 20, 50, 100$ μm, (a) $D_{ew} = 6$ μm, (b) $D_{ew} = 20$ μm.

and thus higher brightness temperature. When the size of water droplets increases to 20 μm, this effect becomes much smaller. At this point, the BTs of the mixed-phase cloud are almost constant for a range of different sizes of ice particles, except for the small ice particle case when $D_{ei} = 10$ μm. When this occurs, it is problematic to retrieve the effective size of the cloud particles from the high-resolution spectral observation. The spectral signature of the mixed-phase cloud also varies substantially when different effective sizes are used for ice crystals (Fig. 13), in particular, when the smaller ice crystals are mixed with large water droplets.

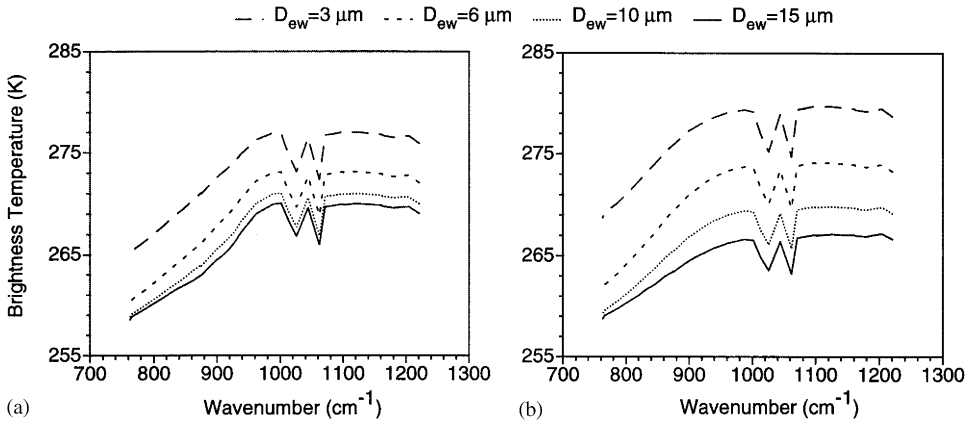

Fig. 13. Same as Fig. 12 except $D_{ew} = 3, 6, 10, 15$ μm, (a) $D_{ei} = 10$ μm, (b) $D_{ei} = 50$ μm.

In general, the spectral radiation of mixed-phase clouds changes with the sizes of both ice crystals and water droplets, and the fraction of ice (γ). The small particles of either ice or water phase have a significant impact on the radiative signature of these clouds when the fraction of ice is constant. Therefore, minor amounts of small water droplets have an important influence on the radiative signature of mixed-phase clouds, and therefore should be considered in the retrieval of the physical and optical properties of cloud residing at temperatures where a mixture of water and ice particles is possible.

5. Summary

The formulae of the single-scattering and absorption properties for mixed-phase clouds are derived from the properties of ice crystals and spherical water droplets. The extinction coefficient for mixed-phase clouds is expressed in the same form as for ice-phase or liquid-phase clouds. The extinction efficiency, absorption efficiency, and asymmetry parameter of mixed-phase clouds and the variations of their effective size and ice fraction ratio are discussed. High-resolution spectral brightness temperature of mixed-phase clouds for different effective sizes, ice fraction ratios, and optical thicknesses have been calculated. We find that the presence of small water droplets has a substantial contribution to the spectral signature of mixed-phase clouds when the fraction ratio of ice is held constant. The spectral signature of mixed-phase clouds are compared to pure ice-phase cirrus, showing that the spectral signature of mixed-phase is quite different from that for cirrus clouds even if a minor amount of small water droplets are included in the mixed-phase cloud layer. This effect should be considered for the retrieval of the mid-level cirrus where the presence of small amounts of liquid water droplets is a possibility.

In addition to the effective size and optical thickness of ice crystals and water droplets as discussed in the paper, other factors such as the ice crystal habits, particle size distribution, cloud height, and cloud temperature may affect the brightness temperature of mixed-phase clouds. The spectral radiative signature of mixed-phase clouds depends on the effective size of ice crystals and water droplets, their single-scattering properties and the aforementioned other factors. For practical applications involving

mixed-phase clouds, further research effort is required to parameterize the infrared radiative properties of these clouds.

Acknowledgements

This study is supported by research grants (NAG-1-02002, NAG5-11374) from the NASA Radiation Sciences Program managed by Dr. Donald Anderson, and is also supported by GIFTS-IOMI MURI project and NASA CLIPSO project.

Appendix A. Effective size and mean asymmetry factor of mixed-phase clouds

Using the definition of the effective mixed-phase cloud that is consistent with that for cirrus clouds (e.g., [25]), we can represent the effective size as a sum of the effective sizes of ice and water components (from Eq. (3)) as follows:

$$D_e = \frac{3}{2}\frac{\int_{L_{min}}^{L_{max}} V_i n_i dL + \int_{r_{min}}^{r_{max}} V_w n_w dr}{\int_{L_{min}}^{L_{max}} A_i n_i dL + \int_{r_{min}}^{r_{max}} A_w n_w dr}. \tag{A.1}$$

Via simple rearrangement of Eq. (4), we get an expression for the integrated volume

$$\int_{L_{min}}^{L_{max}} V_i n_i dL = \frac{IWC}{\rho_i} \tag{A.2}$$

and substituting this expression into Eq. (3) and rearranging yields

$$\int_{L_{min}}^{L_{max}} A_i n_i dL = \frac{3}{2}\frac{\int_{L_{min}}^{L_{max}} V_i n_i dL}{D_{ei}} = \frac{3}{2}\frac{IWC}{D_{ei}\rho_i}. \tag{A.3}$$

Similar expressions for water droplets exist. Substituting Eqs. (A.2) and (A.3) and their corresponding water droplet equations into Eq. (A.1), and using the definition of γ yields Eq. (8).

Using this definition of D_e, the transformation of the sum of the extinction coefficients given in Eq. (1) can be shown to be the simple relation given in Eq. (9). Eq. (1) can be rewritten to express the extinction coefficient β_e as follows:

$$\begin{aligned}\beta_e = \frac{3}{2} &\left(\langle Q_{ei}\rangle \frac{IWC}{D_{ei}\rho_i} + \langle Q_{ew}\rangle \frac{LWC}{D_{ew}\rho_w}\right)\left(\frac{IWC}{D_{ei}\rho_i} + \frac{LWC}{D_{ew}\rho_w}\right)^{-1} \\ &\times \left(\frac{IWC}{D_{ei}\rho_i} + \frac{LWC}{D_{ew}\rho_w}\right)\left(\frac{IWC}{\rho_i} + \frac{LWC}{\rho_w}\right)^{-1} \\ &\times \left(\frac{IWC}{\rho_i} + \frac{LWC}{\rho_w}\right)(IWC + LWC)^{-1} \\ &\times (IWC + LWC).\end{aligned} \tag{A.4}$$

The first term in Eq. (A.4) is the effective extinction efficiency $\langle Q_e \rangle$ of the mixed-phase cloud, as given in Eq. (10). The remaining terms of this equation are $1/D_e, 1/\rho_e$, and *TWC* (Eqs. (6)–(8), respectively).

The derivation of the effective asymmetry parameter $\langle g_e \rangle$ is similar. Starting with the definition of the asymmetry parameter for a two-component cloud, we get

$$\langle g_e \rangle = \frac{\int_{L_{min}}^{L_{max}} g_i(Q_{ei} - Q_{ai})A_i n_i \mathrm{d}L + \int_{r_{min}}^{r_{max}} g_w(Q_{ew} - Q_{aw})A_w n_w \mathrm{d}r}{\int_{L_{min}}^{L_{max}} (Q_{ei} - Q_{ai})A_i n_i \mathrm{d}L + \int_{r_{min}}^{r_{max}} (Q_{ew} - Q_{aw})A_w n_w \mathrm{d}r}. \tag{A.5}$$

Using the following two simple relationships

$$\int_{L_{min}}^{L_{max}} g_i(Q_{ei} - Q_{ai})A_i n_i \mathrm{d}L = \frac{\int_{L_{min}}^{L_{max}} g_i(Q_{ei} - Q_{ai})A_i n_i \mathrm{d}L}{\int_{L_{min}}^{L_{max}} (Q_{ei} - Q_{ai})A_i n_i \mathrm{d}L} \times \int_{L_{min}}^{L_{max}} (Q_{ei} - Q_{ai})A_i n_i \mathrm{d}L = \langle g_i \rangle \int_{L_{min}}^{L_{max}} (Q_{ei} - Q_{ai})A_i n_i \mathrm{d}L \tag{A.6}$$

and

$$\int_{L_{min}}^{L_{max}} (Q_{ei} - Q_{ai})A_i n_i \mathrm{d}L = \frac{\int_{L_{min}}^{L_{max}} (Q_{ei} - Q_{ai})A_i n_i \mathrm{d}L}{\int_{L_{min}}^{L_{max}} A_i n_i \mathrm{d}L} = \langle (Q_{ei} - Q_{ai}) \rangle \frac{3}{2} \frac{IWC}{D_{ei}\rho_i}, \tag{A.7}$$

together with the definition of γ, we get

$$\langle g_e \rangle = \frac{\frac{\langle g_i \rangle \langle (Q_{ei} - Q_{ai}) \rangle \gamma}{D_{ei}\rho_i} + \frac{\langle g_w \rangle \langle (Q_{ew} - Q_{aw}) \rangle (1-\gamma)}{D_{ew}\rho_w}}{\frac{\langle (Q_{ei} - Q_{ai}) \rangle \gamma}{D_{ei}\rho_i} + \frac{\langle (Q_{ew} - Q_{aw}) \rangle (1-\gamma)}{D_{ew}\rho_w}}. \tag{A.8}$$

However,

$$\begin{aligned} &\frac{\langle (Q_{ei} - Q_{ai}) \rangle \gamma}{D_{ei}\rho_i} + \frac{\langle (Q_{ew} - Q_{aw}) \rangle (1-\gamma)}{D_{ew}\rho_w} \\ &= \left(\frac{\langle Q_{ei} \rangle \gamma}{D_{ei}\rho_i} + \frac{\langle Q_{ew} \rangle (1-\gamma)}{D_{ew}\rho_w} \right) - \left(\frac{\langle Q_{ai} \rangle \gamma}{D_{ei}\rho_i} + \frac{\langle Q_{aw} \rangle (1-\gamma)}{D_{ew}\rho_w} \right) \\ &= \frac{\langle (Q_e - Q_a) \rangle}{D_e \rho_e} \end{aligned} \tag{A.9}$$

and substituting Eq. (A.9) into Eq. (A.8) yields, after some manipulation, Eq. (12).

References

[1] Treut HL, Li ZX, Forichon M. Sensitivity of the LMD general circulation model to greenhouse forcing associated with two different cloud water parameterizations. J Climate 1994;7:1827–41.
[2] Sun Z, Shine KP. Studies of radiative of ice and mixed-phase clouds. Q J R Meteorol Soc 1994;120:111–37.
[3] Sun Z, Shine KP. Parameterization of ice clouds radiative properties and its application to potential climatic importance of mixed-phase clouds. J Climate 1995;9:1874–88.
[4] Riley JT. Mixed-phase icing conditions: a review. Technical Report of Federal Aviation Administration, DOT/FAA/AR-98/76, Washington DC, 1998. http://www.tc.faa.gov/its/act141/reportpage.html.
[5] Shupe MD, Uttal T, Matrosov SY, Frisch AS. Clouds water contents and hydrometeor size during the FIRE Arctic Clouds Experiment. J Geophys Res 2001;106:15015–28.
[6] Pinto JO, Curry JA, Intrieri JM. Clouds-aerosol interaction during autumn over Beaufort Sea. J Geophys Res 2001;106:15077–97.
[7] Girard E, Curry JA. Simulation of Arctic low-level clouds observed during the FIRE Arctic Clouds Experiment using a new bulk microphysics scheme. J Geophys Res 2001;106:15139–54.
[8] Young SA, Platt CMR, Austin RT, Patterson GR. Optical properties and phase of some midlatitude, mid-level clouds in ECLIPS. J Appl Meteorol 2000;39:135–53.
[9] Platt CMR, Scott JC, Dilley AC. Remote sounding of high clouds. VI: optical properties of midlatitude and tropical cirrus. J Atmos Sci 1987;44:729–47.
[10] Hogan RJ, Francis PN, Flentje H, Illingworth AJ, Quante A, Pelon J. Characteristics of mixed-phase clouds, Part I: lidar, radar, and aircraft observations from CLARE'98. Q J R Meteorol Soc, 2002, submitted for publication.
[11] Hogan RJ, Illingworth AJ, Poiares Baptista JPV, O'Connor EJ. Characteristics of mixed-phase clouds. Part II: a climatology from ground-based lidar. Q J R Meteorol Soc, 2002, submitted for publication.
[12] Robert M, Tokay A. An explanation for the existence of supercooled water at the top of cold clouds. J Atmos Sci 1991;48:1005–23.
[13] Intrieri JM, Shupe MD, Uttal T, McCarty BJ. An annual cycle of Arctic cloud characteristics observed by radar and lidar at SHEBA. J Geophys Res, 2002, submitted for publication.
[14] Gao BC, Yang P, Han W, Li RR, Wiscombe WJ. An algorithm using visible and 1.38-μm channels to retrieve cirrus cloud reflectances from aircraft and satellite data. IEEE Trans Geosci Remote Sensing 2002;40:1659–68.
[15] Smith WL, Ackerman S, Revercomb H, Huang H, DeSlover DH, Feltz W, Gumley L, Collard A. Infrared spectral absorption of nearly invisible cirrus clouds. Geophys Res Lett 1998;25:1137–40.
[16] Smith WL, Frey R. On clouds altitude determinations from high resolution interferometer sound(HIS) observations. J Appl Meteorol 1990;29:658–62.
[17] Smith WL, Ma XL, Ackerman SA, Revercomb HE, Knuteson RO. Remote sensing clouds properties from high spectral resolution infrared observations. J Atmos Sci 1993;50:1708–20.
[18] Stamnes K, Tsay SC, Wiscombe W, Jayaweera K. A numerically stable algorithm for discrete-ordinate-method radiative transfer in multiple scattering and emitting layered media. Appl Opt 1988;27:2502–9.
[19] Mie G. Beiträge zur Optik trüber Medien, speziell kol-loida-ler Metallösungen. Ann Phys 1908;25:377–446.
[20] Wiscombe WJ. Improved Mie scattering algorithms. Appl Opt 1980;19:1505–9.
[21] Heymsfield AJ, Platt CMR. A parameterization of the particle size spectrum of ice clouds in terms of the ambient temperature and the ice water content. J Atmos Sci 1984;41:846–55.
[22] Heymsfield AJ, Iaquinta J. Cirrus crystal terminal velocities. J Atmos Sci 2000;57:916–38.
[23] Baran AJ, Havemann S. Rapid computation of the optical properties of hexagonal columns using complex angular momentum theory. JQSRT 1999;66:499–519.
[24] Fu Q, Yang P, Sun WB. An accurate parameterization of the infrared radiative properties of cirrus clouds for climate models. J Climate 1998;25:2223–37.
[25] Yang P, Gao BC, Baum BA, Hu YX, Wiscombe WJ, Tsay SC, Winker DM, Nasiri SL. Radiative properties of cirrus clouds in the infrared (8–13 μm) spectral region. JQSRT 2000;70:473–504.
[26] Hansen JE, Travis LD. Light scattering in planetary atmosphere. Space Sci Rev 1974;16:527–610.
[27] Grenfell TC, Warren SG. Representation of nonspherical ice particle by a collection of independent sphere for scattering and absorption of radiation. J Geophys Res 1999;104:31697–709.
[28] Foot JS. Some observations of the optical properties of clouds: II. Cirrus. Q J R Meteorol Soc 1988;114:145–64.

[29] Francis PN, Jones A, Saunders RW, Shine KP, Slingo A, Sun Z. An observational and theoretical study of the radiative properties of cirrus: some results from ICE'89. Q J R Meteorol Soc 1994;120:809–48.
[30] Wyser K, Yang P. A average crystal size and bull shortwave single scattering properties in ice clouds. J Atmos Res 1998;45:315–35.
[31] Fu Q, Sun WB, Yang P. On model of scattering and absorption by cirrus nonspherical ice particles at thermal infrared wavelength. J Atmos Res 1999;56:2937–47.
[32] Arnott WP, Dong YY, Hallett J. Extinction efficiency in the infrared (2–18 μm) of laboratory ice clouds: observations of scattering minimum in the Christiansen bands of ice. Appl Opt 1995;34:541–51.
[33] Yang P, Liou KN, Arnott WP. Extinction efficiency and single-scatttering albedo for laboratory and natural cirrus clouds. J Geophys Res 1997;102:21825–35.
[34] Rothman LS, Rinsland CP, Goldman A, et al. The HITRAN molecular spectroscopic database and HAWKS (HITRAN Atmospheric Workstation): 1996 edition. JQSRT 1998;60:665–710.
[35] Roberts RE, Selby JEA, Biberman LM. Infrared continuum absorption by atmospheric water vapor in the 8–12 μm window. Appl Opt 1976;15:2085–90.
[36] Chung S, Ackerman S, Van Delst PF, Menzel WP. Model calculations and interferometer measurements of ice-clouds characteristics. J Appl Meterol 2000;39:634–44.